IOP Concise Physics

Tying Light in Knots

Applying topology to optics

David S Simon

Chapter 9

Topological states of matter and light

In chapter 1, the role of Dirac monopoles and the Aharonov–Bohm effect in spurring interest in topological aspects of gauge field theories was discussed. In a similar manner, the discovery of the quantum Hall effect soon led to a variety of related phenomena whose explanations also turned out to rely heavily on topological effects. Among these phenomena are the discovery of electron states that propagate unidirectionally without scattering at impurities and that propagate only on the surface of a material, not in the interior. Such states are characterized by integer-valued topological invariants such as winding number or Chern numbers.

More recently, it has been realized that similar phenomena can be achieved with photons in optical systems, and that optical systems can in fact be used to simulate nontrivial topological behavior of condensed matter and other systems.

We begin in the next two sections by reviewing the quantum Hall effect and other topological effects in condensed matter systems. In the final section, we give a brief description of how similar topological phenomena can arise in connection with motions of photons through optical systems.

9.1 The quantum hall effect

The *classical Hall effect*, in which the presence of a static *magnetic* field causes the appearance of an *electric* potential difference, was discovered in 1879 by Edwin Hall while he was a graduate student at Johns Hopkins. The Hall effect forms the basis for numerous types of high-precision measurements and sensing devices.

Consider a conductor carrying a current along the x-axis in the presence of a uniform magnetic field pointing along the z-axis, as in figure 9.1. Let w and L be the widths in the y- and z-directions, respectively. The charge carriers (electrons) move opposite to the current direction and feel a magnetic force $\boldsymbol{F}_B = -e\boldsymbol{v} \times \boldsymbol{B}$ in the y-direction. As a result, electrons start to accumulate on one side of the material, while a deficit of electrons creates an effective buildup of positive charge on the other side. The charge separation causes an electric field $\boldsymbol{E}_x$ to grow, pointing toward the

doi:10.1088/2053-2571/aaddd5ch9

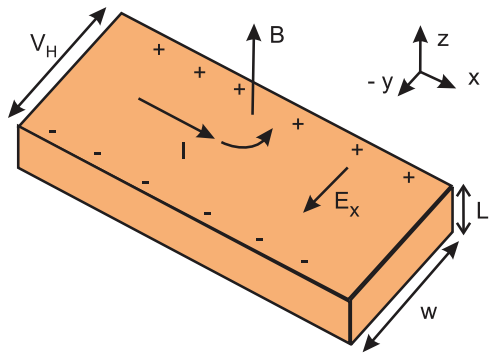

Figure 9.1. The classical Hall effect. The magnetic field deflects the current, causing a buildup of charges on the sides of the material. The separated charges then cause an electric field and a voltage difference in the direction transverse to the current.

left (from the positive charge toward the negative). This field then causes an electric force $\boldsymbol{F}_E = -e\boldsymbol{E}_x$ opposed to $\boldsymbol{F}_B$. The charge on the edges of the material continue to accumulate until it is sufficiently large for the electric and magnetic forces to cancel:

$$-eE_x = -e|\boldsymbol{v} \times \boldsymbol{B}| \quad \rightarrow \quad E_x = vB. \tag{9.1}$$

At this point, equilibrium is reached, with the charges on the edges of the conductor creating a voltage difference across the material in the y-direction,

$$V_H = E_x w = evBw. \tag{9.2}$$

This voltage is known as the *Hall voltage*, and is easily measured by connecting a voltmeter across the two sides of the conductor.

The Hall voltage can be put into a more useful form. The current can be written in terms of the electron density (number of electrons per volume) n as $I = nevA = nevwL$, where $A = wL$ is the area in the y–z plane. So the Hall voltage can be written in terms of the current as

$$V_H = \frac{BI}{nL}. \tag{9.3}$$

In addition to the usual Ohm's law resistance $R_{xx} = \frac{V_0}{I}$ (in this context referred to as the *longitudinal resistance*), we may also define a *transverse resistance*

$$R_{xy} = \frac{V_H}{I}. \tag{9.4}$$

This resistance may seem a bit odd at first: it is measuring the ratio of the voltage in the y-direction to the current in the x-direction. Since the experimenter usually controls the value of B, and the height L of the material is easy to measure, the measurement of the Hall resistance provides an accurate way of determining the electron density n in the material. Alternatively, if the charge carrier density of the material is well known, then the Hall effect provides a means of making precise measurements of the magnetic field.

The magnetic field causes the electrons to undergo circular motion (figure 9.2) in the x–y plane at the cyclotron frequency,

$$\omega = \frac{eB}{m} \tag{9.5}$$

Note, however, what happens at the edges: the circle cannot be completed without running into the edge and reflecting. This leads to the skipping motion shown in figure 9.2. The result is that the bulk of the conduction occurs only at the boundaries, and current conducts in only one direction at each boundary.

Consider now a two-dimensional system in the x–y plane, with negligible thickness in the z-direction. The current density in two dimensions is defined to be the current per length (instead of per area as in three dimensions), $J = I/w$. The resistivity of the material is defined to be

$$\boldsymbol{J} = \sigma \boldsymbol{E}, \tag{9.6}$$

where the conductivity σ is a tensor described by a two-by-two matrix:

$$\sigma = \begin{pmatrix} \sigma_{xx} & \sigma_{xy} \\ -\sigma_{xy} & \sigma_{xx} \end{pmatrix}. \tag{9.7}$$

The resistivity is given by the inverse of the conductivity:

$$\rho = \sigma^{-1} = \begin{pmatrix} \rho_{xx} & \rho_{xy} \\ -\rho_{xy} & \rho_{yy} \end{pmatrix}. \tag{9.8}$$

The matrices are easy to invert, giving

$$\sigma_{xx} = \frac{\rho_{xx}}{\rho_{xx}^2 + \rho_{xy}^2}, \qquad \sigma_{xy} = -\frac{\rho_{xy}}{\rho_{xx}^2 + \rho_{xy}^2}. \tag{9.9}$$

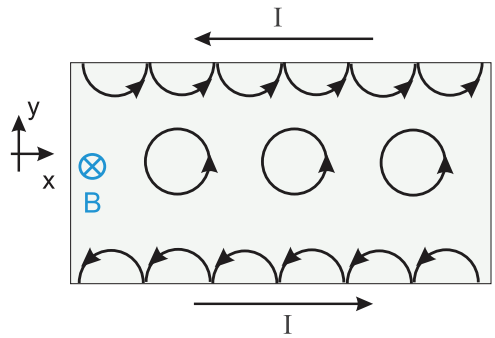

Figure 9.2. Motion of electrons in a magnetic field. In the bulk, the magnetic force causes circular motions. Near the edges, the circular motions are interrupted by collisions with boundary. This leads to unidirectional skipping motion along each edge. Note that the motion is in opposite directions on each of the two edges.

It should be noted that in the two-dimensional context, there is no distinction between resistance and resistivity; for example, since $V_H = -wE_x$ and $I = wJ_y$, it is seen that

$$R_{xy} = \frac{V_H}{I} = -\frac{E_x}{J_y} = -\rho_{xy}, \tag{9.10}$$

where the minus signs indicate that V_H increases opposite to the direction of $\boldsymbol{E}_x$. The *Hall coefficient* is then defined as

$$R_H = -\frac{E_x}{J_y B} = \frac{\rho_{xy}}{B}. \tag{9.11}$$

It is straightforward to compute the various quantities just defined by means of the *Drude* or *free-electron model* [1–3] of solid state physics. In particular, the model predicts that:

$$\rho_{xx} = \frac{m}{ne^2\tau}, \qquad \rho_{xy} = -\frac{B}{ne}, \qquad R_H = \frac{1}{ne}, \tag{9.12}$$

where m, n, and τ are, respectively, the electron mass, electron density, and scattering time in the material. Notice in particular that in this classical model, the Hall resistance is a continuous, linear function of magnetic field B.

The *integer quantum Hall effect* was discovered in 1980 [4]. The effect occurs in thin films (of thickness no more than 5–10 nm) and other systems where the electrons have little freedom to move in one direction, leaving an effective two-dimensional system. In the presence of a magnetic field perpendicular to the 2D system, electrons exhibit cyclotron motion, as above. At room temperature, these motions are disrupted by thermal noise, but at very low temperatures (<1 K) and strong magnetic fields the thermal scattering time is much longer than the orbital period, leaving the circular motions largely undisturbed. The energies of the cyclotron orbits are quantized, leading to a series of discrete energy levels $E_\nu = \left(\nu + \frac{1}{2}\right)\hbar\omega$, called *Landau levels* (with $\nu = 1, 2, \ldots$). Under these conditions, the Hall resistance R_H exhibits a series of plateaus as a function of magnetic field strength (figure 9.3(a)), in contrast to the classical effect, where R_H is a simple linear function of B (equation (9.4)). The plateaus appear at the values

$$R_H = \frac{h}{\nu e^2} \approx \frac{25812.8\ \Omega}{\nu}, \tag{9.13}$$

where $\nu = 2, 3, 4, \ldots$. While on these plateaus, the ordinary (non-Hall) resistance of the material vanishes. The transverse conductivity is found to be quantized:

$$\sigma_{xy} = \frac{e^2}{h}\nu. \tag{9.14}$$

The plateaus occur because the Landau levels are quantized: increasing B cannot affect R_H until it contributes enough energy to promote an electron to the next higher Landau level.

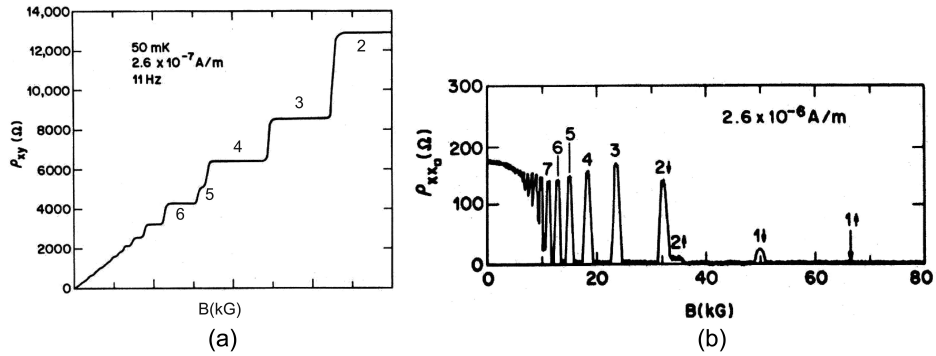

Figure 9.3. The integer quantum Hall effect. (a) As the magnetic field is increased, the Hall resistance exhibits plateaus. Each plateau is characterized by an integer value of $\frac{h}{R_H e^2}$ or $\frac{\sigma h}{e^2}$. (b) The longitudinal resistivity along the direction of the E field vanishes on the plateaus, spiking at the points where the jumps between plateaus occur. (Figures reproduced with permission from [5], with additional labels added.) Copyright (1982) by the American Physical Society.

Each plateau is centered at the field value

$$B = \frac{2\pi\hbar n}{\nu e} \equiv \frac{n}{\nu}\Phi_0, \tag{9.15}$$

where n is the electron density, $\Phi_0 = \frac{2\pi\hbar}{e}$ is the fundamental flux quantum, and ν is a positive integer. The resistivities of the plateaus are characterized by the same integers,

$$\rho_{xy} = \frac{2\pi\hbar}{e^2\nu}. \tag{9.16}$$

The presence of the integer ν, is a reflection of the topological origin of the integer quantum Hall effect.

On each plateau, the longitudinal resistivity ρ_{xx} vanishes, while $\rho_{xy} \neq 0$. This leads to an odd effect: according to equation (9.9), this implies that σ_{xx} also vanishes: the longitudinal resistivity and conductivity both vanish simultaneously!

The integer quantum Hall effect is prominent in impure or disordered material samples. As the sample becomes purer, the integer plateaus become less prominent, and eventually disappear. As this happens, a new effect becomes apparent: plateaus at fractional values begin to become noticeable. This *fractional quantum Hall effect* was discovered in semiconductor materials in 1982 [6, 7]. The plateaus now occur at $R_H = \frac{h}{e^2}\alpha$, where α takes on simple fractional values such as $\alpha = \frac{1}{3}, \frac{1}{5}, \frac{1}{7}, \frac{2}{3}, \frac{4}{5}, \ldots$. Experimentally, the most prominent plateaus occur at $\alpha = 1/3$ and $\alpha = 2/5$. In contrast to the integer effect, which occurs even if the interactions between electrons are ignored, the fractional effect is dependent on the presence of electron–electron interactions.

The transverse Hall conductivity is of topological origin. At each point in the two-dimensional Brillouin zone, it turns out that

$$\sigma_{xy}(\boldsymbol{k}) = \frac{e^2}{\hbar} F_{\mu\nu}, \tag{9.17}$$

where $F_{\mu\nu} = \partial_{k_x} A_y - \partial_{k_y} A_x$ is the curvature of a Berry potential $\boldsymbol{A}$. The Brillouin zone is a torus, T^2 in momentum space, so the value of σ_{xy} averaged over the zone is

$$\sigma_{xy} = \frac{1}{(2\pi)^2} \int_0^{2\pi} \int_0^{2\pi} \sigma_{xy}(\boldsymbol{k}) dk_x dk_y = \frac{e^2}{(2\pi)h} \int_{T^2} F_{\mu\nu} d^2k = \frac{e^2}{h} c_1, \tag{9.18}$$

where c_1 is the first Chern number defined in equation (5.13). In this context, the Chern number on the Brillouin zone is referred to as the TKNN invariant [8].

Further odd effects occur in the fractional quantum Hall effect. For example, the charge carriers are 'fractionalized': screening of charges leads to the electrons seeming to have parts of their charge in different, widely separated locations. Similarly, the quantum mechanical statistics become fractional. In three dimensions all particles must have integer or half-integer spin, leading to bosonic or fermionic behavior, respectively. But in two dimensions, the spin can effectively have a continuous range of values, continuously interpolating between boson and fermion behavior. Such fractional-statistics particles are called *anyons*.

The relevance of the Chern number here is due to the following. The Hamiltonian is a matrix-valued function on the two-dimensional Brillouin zone parameterized by the two components of the momentum, k_x and k_y. Because of the periodicity of the lattice, these components are both periodic; thus, the Brillouin zone is actually a torus, T^2. Meanwhile, the spin state of the electron at fixed k is given by a point on the Bloch sphere, S^2. There is thus a map from the torus to the sphere. These are classified by the homotopy groups of bundles of states over tori, which are indexed by an integer, the Chern number. The system is described by a fiber bundle with base given by the torus and fiber given by the Bloch sphere which describes the possible spin states.

Topological effects can also occur in one-dimensional systems as well. In this case, the relevant topological invariant becomes the winding number.

Other variations on the quantum Hall effect can occur. In 1988, Haldane [9] showed that a Hall-like effect can occur in periodic systems in the absence of Landau levels, providing a quantum version of an effect first seen in classical systems by Hall in 1880. This *anomalous quantum Hall effect* was seen experimentally in 2013 [10]. As another example, note that the quantum Hall effect can be viewed as a unidirectional charge pump: charge is transported in a single direction, with no charge flowing the other way; a similar effect, known as the *spin quantum Hall effect*, acts as a one-way pump for spin [11–13].

Materials that exhibit the quantum Hall effect are examples of a more general category of materials called *topological insulators*, materials that are insulating in their bulk but conduct unidirectionally on their boundaries. The surface currents are immune to backscattering at impurities, and so the currents are very robust. These materials are currently objects of intense interest, both because of their

unique physical properties and because of their applications for quantum information processing and other areas.

More detailed reviews of quantum Hall effects may be found in [14–17]. Reviews of topological insulators and the related topic of topological superconductors include [18–21].

9.2 Topological phases and localized boundary states

As the momentum of a one-dimensional crystal or other periodic system is varied over a full Brillouin zone, the momentum–space Hamiltonian $\hat{H}(\boldsymbol{k})$ traces out a closed loop in the space of Hermitian matrices. For the systems of interest here, the loop will lie on the intersection of a plane and the Bloch sphere. The winding number counts the number of times the loop encloses the singular point of the Hamiltonian at the origin, where all of the energies collapse to zero. In the case of a two-dimensional system, the values of k will lie on a torus and $\hat{H}(\boldsymbol{k})$ will define a mapping of the torus to the Bloch sphere; the topological invariant associated with this mapping will be a Chern number.

Topological insulators have energy levels or energy bands that are separated by finite gaps (figure 9.4(a)). The size of the gap varies as k traverses the Brillouin zone, but should remain nonzero to avoid the singularity. Topological invariants can only change when the energy gap closes; in analogy with the optical vortices of chapter 6, topological invariants can only change when the loops or spheres that define them cross the singular point. The wavefunctions in each energy band form a fiber bundle over the Brillouin, and the topological invariants measure the topological non-triviality of the bundle.

For the sake of specificity, let us assume henceforth that we are dealing with two-dimensional systems; in other words, three-dimensional objects in which one direction is of negligible thickness. A common example is graphene, which forms two-dimensional layers that are only a single atom thick.

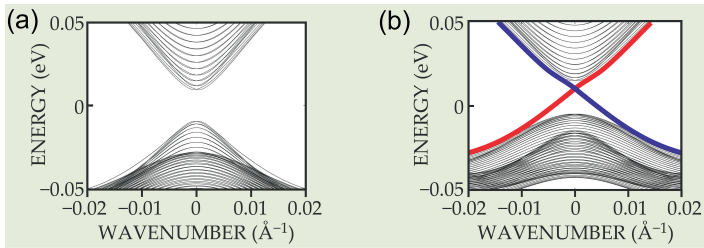

Figure 9.4. (a) In topological insulators, finite energy gaps are maintained between bands. Topological invariants such as the Chern number can only change when the gap closes. (b) When two materials with different Chern number are brought together, new states appear at the boundary that can cross between the bands. These states are highly localized and highly stable: topological considerations prevent them from being destroyed by continuous changes of the system parameters. (Figure reproduced from [13].)

Suppose that a pair of two-dimensional crystals, M_1 and M_2, of different Chern number $c_1(M_1) \neq c_2(M_2)$, are brought into contact. Then it is found that a new quantum state arises, which is highly localized near the one-dimensional boundary in the sense that it decays rapidly as you move away in either direction. These *boundary* or *edge states* interpolate between the solutions on the two sides, and only appear when the gap between energy bands vanishes. These zero-energy states are topological solitons, and they are of great interest for information processing and other applications because they are extremely robust: they are defined by the global properties of the system and cannot be destroyed by continuous perturbations of the system's Hamiltonian. The states are said to be *topologically protected.*

There are two types of boundary states: one whose energy crosses zero in the positive direction (going from the lower energy valence band to the higher energy conduction band as the electron moves from left to right) and those that cross zero in the negative direction (figure 9.4(a)). Let $N_{\pm}$ represent the numbers of these two types of states. We can define a type of topological index for this system,

$$\nu = N_+ - N_-. \tag{9.19}$$

Then a fundamental result is the bulk–boundary correspondence:

$$\nu = c_1(M_2) - c_1(M_1). \tag{9.20}$$

In other words, the number of boundary states going in each direction must equal the change in Chern number across the boundary.

9.3 Topological photonics

So far in this chapter we have discussed electrons in solids, rather than photons in optical systems. But similar topologically based effects have recently been shown to appear in optics and photonics [22–24], and in these cases many of the results of the previous sections will apply with only minor changes. In this setting, a Berry curvature often plays the role of the magnetic field. In the remainder of this section we give a very brief overview of this new area of topological photonics; consult the references for further detail.

In 2005, Haldane and Raghu [25, 26] pointed out that an analog of the anomalous quantum Hall effect can be produced in optical systems. The system they discussed was a *photonic crystal* [27], a periodic lattice through which light propagates. There are gaps between the frequencies that propagate without reflection, similar to the electron band gaps in solids. It was predicted that two-dimensional systems with Hamiltonians of nontrivial Chern number could exist. These would display unidirectional edge states which would persist even in the presence of high levels of impurities or disorder; there would be no allowed states running in the other direction into which photons could scatter. When two of these systems in different topological phases are brought together, there would be boundary states trapped between them along the boundary between different Chern numbers. These predictions were soon verified experimentally [28, 29].

Similar topologically based effects have since been demonstrated in a range of other systems [30–35], including optical cavities, quasicrystals, and lattices of coupled optical oscillators. Photonic edge states were first seen in microwave systems [29], but have now been detected in a variety of frequency ranges.

The existence of the quantum Hall effect depends on the breaking of time reversal symmetry by the presence of a magnetic field. It was soon found that the presence or absence of parity-reversal symmetry, particle–hole symmetry and of chiral symmetry (symmetry under interchange of two distinct types of lattice sites) are also relevant to the existence of topological phases. A classification of topological states possible with or without each of these symmetries has been constructed [36, 37] and is often referred to as the periodic table of topological insulators. Various mechanisms have been used to create symmetry conditions that allow the existence of topological states in photonics; for example, nonlinear devices called Faraday rotators can be used to break time reversal symmetry [38], or the light can be sent into bipartite optical systems in which two distinct types of optical components alternate to create a chiral symmetry. The latter approach allows topological states to appear, for example, in cold atom optical lattices and in photonic quantum walk systems.

Quantum walks of photons on discrete lattices [39] are especially attractive because of their relative simplicity in experimental terms. In a *classical random walk* [40], a particle lives on some discrete lattice (which we will assume to be one-dimensional for simplicity) and at each multiple of some discrete time T the particle jumps either left or right from its current location to one of the adjacent sites. The probability to jump right is some fixed value p, while the probability to jump left is $q = 1 - p$. As shown in every introductory statistical mechanics text [41–43], the probability of being at lattice site m after N time steps is given by a binomial distribution (see figure 9.5(a)),

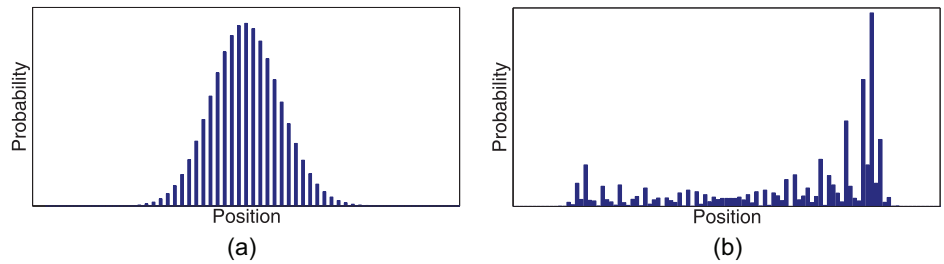

Figure 9.5. (a) Classical random walk. The particle starts in the middle and has fixed probabilities to go left or right at each step. After N steps the probability distribution for positions is binomial and (for large N) approximately Gaussian. The spread is diffusive over time, $\sim\sqrt{N}$. The gaps at every other position are due to the fact that after an even number of steps only even positions can be reached (and similarly for odd positions after odd numbers of steps). (b) Quantum walk. The spread is now ballistic in time, $\sim N$. The asymmetry is due to the choice of coin variable used; more symmetric walks can be produced with other coins. Here, pairs of adjacent positions were lumped together in a single bin to eliminate the gaps at odd sites.

$$P(m) = \frac{N!}{\left(\frac{N+m}{2}\right)!\left(\frac{N-m}{2}\right)!} p^{\frac{N+m}{2}} q^{\frac{N-m}{2}}. \tag{9.21}$$

When N is large, this becomes approximately Gaussian, as required by the central limit theorem. The width of the distribution as measured by the standard deviation grows proportionally to the square root of the time,

$$\sigma \sim \sqrt{N}. \tag{9.22}$$

This square root dependence on time is characteristic of diffusion processes, and so is called *diffusive spread*.

The behavior of *quantum walks* is very different [44–47]. In a quantum walk, there is a wavefunction instead of a classical particle. The wavefunction has both an amplitude to jump left *and* to jump right at each step, so the wavefunction spreads in both directions with each step. The amplitudes for going left or right can be determined by the value of a random variable called the *coin variable*. Another way to consider the process is to use the *Feynman path integral approach* [48] and to think of an ensemble of classical particles; then the wavefunction is to be constructed by adding the amplitudes corresponding to all possible paths of these classical particles. Either way, the amplitudes $a(m)$ for the particle to be at each site evolve deterministically over time and interfere with each other in a complicated manner, so that the final probability distribution is much more complex than in the classical case. The probability of being at site m at time N is then given by the absolute square of the probability amplitude, $P(m) = |a(m)|^2$. The probability distribution for a typical example is shown in figure 9.5(b). One difference is immediately apparent: the distribution is clearly non-Gaussian; in fact the probability tends to be small near the middle and largest at the edges. This is reflected in the behavior of the standard deviation over time: the width after N steps is now given by

$$\sigma \sim N. \tag{9.23}$$

The probability maxima near the edges move linearly in time like a freely propagating classical particle shot from a gun. For this reason, this behavior is called *ballistic spread*.

Quantum walks are of great interest in quantum information processing [49–51] because of that last fact: since the quantum walk spreads faster than any classical random walk, the quantum walk can provide physical implementations of quantum search algorithms and other procedures that operate much faster than the corresponding classical algorithms. This is common in quantum computing, where the superposition principle, interference, and other quantum properties lead to a so-called *quantum speed-up* [52, 53]. Holonomy and Berry phase play important roles in quantum walks; a discussion of this can be found in [54].

It has been demonstrated experimentally [55, 56] that quantum walks of photons in an optical system can simulate the behavior of Hamiltonians with nontrivial

winding number, and that by bringing two such systems of different winding number together topologically protected optical boundary states can be formed. This has been done using two-dimensional arrays of beam splitters and phase plates, with the photon moving along one axis and exhibiting a one-dimensional quantum walk along the perpendicular axis (figure 9.6). Another scheme which allows similar effects in a one-dimensional optical setup has also been proposed [57]. By adding one more dimension to the walk, systems of nontrivial Chern number can also be produced.

Many applications of topological photonic states have been proposed. For example, boundary states along one-dimensional curves could be used as topologically protected waveguides for optical states (figure 9.7). But topological photonics is a new field whose potential has only begun to be explored in the past few years; it is clear that many exciting new effects and applications are bound to arise in coming years.

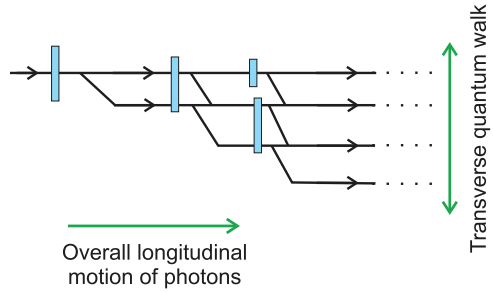

Figure 9.6. An optical implementation of a quantum walk. The random coin operation is carried out by rotating polarization states using half-wave plates (blue rectangles), then separating polarization components using birefringent elements (at the splitting points of the lines). The rotation sizes alternate to create nontrivial topological phases. The photons move left to right, but exhibit a quantum walk in the vertical direction.

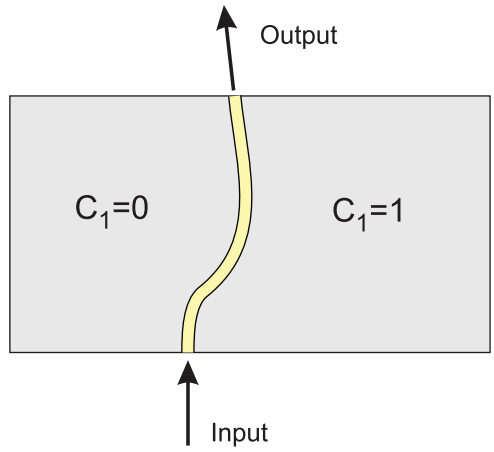

Figure 9.7. Two materials of different topological phases (different Chern numbers) are brought into contact, producing a state localized on the boundary (the yellow curve). The boundary can be used as a waveguide for optical states, with the topological protection serving to keep the state from being degraded by environmental factors.

References

[1] Ashcroft N and Mermin D 1976 *Solid State Physics* (Pacific Grove, CA: Brooks Cole)
[2] Omar M A 1975 *Elementary Solid State Physics* (Reading: Addison-Wesley)
[3] Griffiths D J 2017 *Introduction to Electrodynamics* 4th edn (Cambridge: Cambridge University Press)
[4] von Klitzing K, Dorda G and Pepper M 1980 *Phys. Rev. Lett.* **45** 494
[5] Paalanen M A, Tsui D C and Gossard A C 1982 *Phys. Rev.* B **25** 5566
[6] Tsui D C, Stormer H L and Gossard A C 1982 *Phys. Rev. Lett.* **48** 1559
[7] Laughlin R B 1983 *Phys. Rev. Lett.* **50** 1395
[8] Thouless D, Kohomoto M, Nightingale M and den Nijs M 1982 *Phys. Rev. Lett.* **49** 405
[9] Haldane F D M 1988 *Phys. Rev. Lett.* **61** 2015
[10] Chang C Z *et al* 2013 *Science* **340** 167
[11] Kane C L and Mele E J 2005 *Phys. Rev. Lett.* **95** 226081
[12] Maciejko J, Hughes T L and Zhang S C 2011 *Annu. Rev. Condens. Matter Phys.* **2** 31
[13] Qi X L and Zhang S C 2010 *Phys. Today* **63** 33
[14] Girvin S M 2000 *Topological Aspects of Low Dimensional Systems* ed A Comtet, T Jolicoeur, S Ouvry and F David (Berlin: Springer)
[15] Taylor P L and Heinonen O 2002 *A Quantum Approach to Condensed Matter Physics* (Cambridge: Cambridge University Press)
[16] Goerbig M O 2009 arXiv: 0909.1998v2 [cond-mat.mes-hall]
[17] Tong D 2016 arXiv: 1606.06687 [hep-th]
[18] Stanescu T D 2017 *Introduction to Topological Quantum Matter and Quantum Computation* (Boca Raton, FL: CRC Press)
[19] Bernevig B A(with Hughes T L) 2013 *Topological Insulators and Topological Superconductors* (Princeton, NJ: Princeton University Press)
[20] Hasan M Z and Kane C L 2010 *Rev. Mod. Phys.* **82** 3045
[21] Asbóth J K, Oroszlány L and Pályi A P 2017 *A Short Course on Topological Insulators: Band Structure and Edge States in One and Two Dimensions* (Heidelberg: Springer)
[22] Lu L, Joannopoulos J D and Soljačić M 2014 *Nat. Photon.* **8** 821
[23] Khanikaev A B and Shvets G 2017 *Nat. Photon.* **11** 763
[24] Kitagawa T 2012 *Quantum Inf. Process.* **11** 1107
[25] Haldane F D M and Raghu S 2008 *Phys. Rev. Lett.* **100** 013904
[26] Raghu S and Haldane F D M 2008 *Phys. Rev.* A **78** 033834
[27] Joannopoulos J, Johnson S, Winn J and Meade R 2008 *Photonic Crystals: Molding the Flow of Light* (Princeton, NJ: Princeton University Press)
[28] Wang Z, Chong Y D, Joannopoulos J D and Soljačić M 2008 *Phys. Rev. Lett.* **100** 013905
[29] Wang Z, Chong Y, Joannopoulos J D and Soljačić M 2009 *Nature* **461** 772
[30] Cho J, Angelakis D G and Bose S 2008 *Phys. Rev. Lett.* **101** 246809
[31] Fang K, Yu Z and Fan S 2011 *Phys. Rev.* B **84** 075477
[32] Liu K, Shen L and He S 2012 *Opt. Lett.* **37** 4110
[33] Hafezi M, Demler E A, Lukin M D and Taylor J M 2011 *Nat. Phys.* **7** 907
[34] Kraus Y E, Lahini Y, Ringel Z, Verbin M and Zilberberg O 2012 *Phys. Rev. Lett.* **109** 106402
[35] Hafezi M, Mittal S, Fan J, Migdall A and Taylor J M 2013 *Nat. Photon.* **7** 1001
[36] Schnyder A P, Ryu S, Furusaki A and Ludwig A W W 2008 *Phys. Rev.* B **78** 195125
[37] Kitaev A 2009 *AIP Conf. Proc.* **1134** 22

[38] Koch J, Houck A A, Hur K and Girvin S M 2010 *Phys. Rev.* A **82** 043811
[39] Tarasinski B, Asbóth J K and Dahlhaus J P 2014 *Phys. Rev.* A **89** 042327
[40] Klafter J and Sokolov M 2011 *First Steps in Random Walks* (Oxford: Oxford University Press)
[41] Reif F 1965 *Fundamentals of Statistical and Thermal Physics* (Long Grove, IL: Waveland Press)
[42] Kittel C 1958 *Elementary Statistical Physics* (Mineola, NY: Dover)
[43] Gould H and Tobochnik J 2010 *Statistical and Thermal Physics: With Computer Applications* (Princeton, NJ: Princeton University Press)
[44] Aharonov Y, Davidovich L and Zagury N 1993 *Phys. Rev.* A **48** 1687
[45] Kempe J 2003 *Contemp. Phys.* **44** 307
[46] Venegas-Andraca S E 2012 *Quantum Inf. Process.* **11** 1015
[47] Manouchehri K and Wang J 2014 *Physical Implementation of Quantum Walks* (Berlin: Springer)
[48] Feynman R P and Hibbs A R 1965 *Quantum Mechanics and Path Integrals* (New York: McGraw-Hill)
[49] Ambainis A 2003 *Int. J. Quant. Inf.* **1** 507
[50] Portugal R 2013 *Quantum Walks and Search Algorithms* (Berlin: Springer)
[51] Venegas-Andraca S E 2008 *Quantum Walks for Computer Scientists* (San Rafael, CA: Morgan and Claypool)
[52] Nielsen M A and Chuang I L 2000 *Quantum Computation and Quantum Information* (Cambridge: Cambridge University Press)
[53] Mermin N D 2007 *Quantum Computer Science: An Introduction* (Cambridge: Cambridge University Press)
[54] Puentes G 2017 *Crystals* **7** 122
[55] Broome M A, Fedrizzi A, Lanyon B P, Kassal I, Aspuru-Guzik A and White A G 2010 *Phys. Rev. Lett.* **104** 153602
[56] Kitagawa T, Broome M, Fedrizzi A, Rudner M S, Berg E, Kassal I, Aspuru-Guzik A, Demler E and White A G 2012 *Nat. Commun.* **3** 882
[57] Simon D S, Fitzpatrick C A, Osawa S and Sergienko A V 2017 *Phys. Rev.* A **96** 013858